Trypanosoma brucei Pex13.2 is an accessory peroxin that functions in the import of PTS2 proteins and localizes to subdomains of the glycosome

Logan P. Crowe[1], Kathleen R. Nicholson[2], Christina L. Wilkinson[1], and Meredith T. Morris[1,3]

[1] Eukaryotic Innovations Center, Department of Genetics and Biochemistry, Clemson University, Clemson, SC 29631

[2] Current address. Department of Biological Sciences, Eck Institute for Global Health, Center for Rare and Neglected Diseases, University of Notre Dame, Notre Dame, IN 46556

[3] Corresponding author

ABSTRACT

Kinetoplastid parasites including *Trypanosoma brucei*, *Trypanosoma cruzi* and *Leishmania* harbor unique organelles known as glycosomes, which are evolutionarily related to peroxisomes. Glycosome/peroxisome biogenesis is mediated by proteins called peroxins that facilitate organelle formation, proliferation and degradation, and import of proteins housed therein. Import of matrix proteins occurs via one of two pathways that are dictated by their peroxisome targeting sequence (PTS). In PTS1 import, a C-terminal tripeptide sequence, most commonly SKL, is recognized by the soluble receptor Pex5. In PTS2 import, a less conserved N-terminal sequence is recognized by Pex7. The soluble receptors deliver their cargo to the import channel consisting minimally of Pex13 and Pex14. While much of the import process is conserved, kinetoplastids are the only organisms to have two Pex13s, *Tb*Pex13.1 and *Tb*Pex13.2. In previous studies, GFP-tagged *Tb*Pex13.1 localized to glycosomes and silencing either protein in the stage of the parasite that lives in the mammalian bloodstream impaired glycosome protein import and slowed parasite growth. While these findings suggest Pex13s are involved in protein import, the mechanisms by which they function are unknown and it is unclear why kinetoplastids would require two Pex13s. In this work, we demonstrate that *Tb*Pex13.2 is associated with the glycosome membrane with its N-terminus facing the cytoplasm. Super-resolution microscopy reveals that *Tb*Pex13.2 localizes to a few (1-3) foci per glycosome and import of PTS2 proteins was disrupted in *Tb*Pex13.2-deficient cells suggesting it may be an accessory factor for PTS2 import.

41 **INTRODUCTION**

42

43 The family Kinetoplastea includes a number of medically relevant parasites including
44 *Trypanosoma brucei*, *Trypanosoma cruzi* and several species of *Leishmania* that cause human
45 African trypanosomiasis, Chagas disease, and several forms of leishmaniasis. Treatments for
46 these diseases are expensive, toxic, and difficult to administer. Additionally, the growing
47 resistance to current therapies necessitates the need for the identification of new drug targets.

48

49 All kinetoplastids have unique membrane-bounded microbodies called glycosomes that are
50 evolutionarily related to peroxisomes of higher eukaryotes (*1*, *2*). Peroxisomes and glycosomes
51 lack DNA and import most matrix proteins post-translationally (*2*). Glycosomes are unique in that
52 they harbor many of the enzymes in the glycolytic pathway, which are cytosolic in higher
53 eukaryotes (*3*–*5*). The essential nature of these organelles makes them a good drug target.
54 Studies demonstrate that small molecules, which interrupt protein import into glycosomes, were
55 lethal to *T. brucei* (*6*).

56

57 Peroxisome biogenesis is regulated by proteins called peroxins (PEXs) that govern organelle
58 formation, proliferation and degradation, as well as protein import (*2*, *3*, *7*). Import of proteins
59 into peroxisomes involves binding of soluble receptor proteins, either Pex5 or Pex7, to a targeting
60 sequence in the cargo protein (*8*, *9*). Pex5 binds to a C-terminal tripeptide with the consensus
61 sequence of SKL called a peroxisome targeting sequence 1 (PTS1) while Pex7 binds to a less
62 conserved N-terminal sequence termed PTS2 (*2*, *10*, *11*). The receptor-cargo complex then
63 docks at the peroxisome membrane through interactions with the glycosome membrane proteins
64 Pex13 and Pex14, which make up the import channel (*12*). After import, the receptors are
65 recycled via a ubiquitination process involving Pex2, 10, and 12 (*13*).

66

67 While much of the import pathway is conserved, kinetoplastids are unique in that they have two
68 Pex13s, which have been designated *Tb*Pex13.1 and *Tb*Pex13.2 (*14*, *15*). These proteins share
69 low sequence identity with each other or with Pex13s from higher eukaryotes. In previous studies,
70 *Tb*Pex13.1, which was the first identified, localized to glycosomes. Silencing of the protein in the
71 mammalian bloodstream (BSF) and insect stage, procyclic form (PCF) parasites yielded parasites
72 with glycosome protein import defects and slowed growth rates (*15*). Later, iterative database
73 searches resulted in the identification of *Tb*Pex13.2 (*14*). Silencing of this second Pex13 via
74 RNA interference in BSF parasites resulted in mislocalization of *Tb*Pex14 and *Tb*aldolase and a
75 defect in growth rate. Prior to our work, *Tb*Pex13.2 RNAi cells lines could not be established in
76 PCF parasites (*14*).
77
78 In pursuit of understanding function, we confirmed that native *Tb*Pex13.2 is an integral glycosome
79 membrane protein and demonstrate that its N-terminus is on the cytoplasmic side of the
80 membrane. Super-resolution microscopy reveals that *Tb*Pex13.2 localization is restricted to a
81 few foci (1-3)/organelle and *Tb*Pex13.2-deficient PCF parasites exhibit a defect in PTS2 import,
82 suggesting that it may serve as a co-receptor in PTS2 import.
83

84 **MATERIALS AND METHODS**

85

86 **Cell culture and transfection of *T. brucei*:** Procyclic form (PCF) 2913 and bloodstream form
87 (BSF) 9013 expressing T7 polymerase and tetracycline (tet) repressor (*16*) were maintained in
88 SDM79 (or the minimal glucose medium SDM79θ containing 5 μM glucose) (*17*) and HMI-9,
89 respectively. Expression vectors for epitope-tagged proteins were generated by cloning the open
90 reading frame of *Tb*Pex13.2 into the pXS2 (PCF) vector or pXS6 (BSF) vectors possessing either
91 a blasticidin resistance or puromycin resistance gene (*18*). For transfection, 20 μg plasmid DNA
92 was linearized (pXS2, pXS6: MluI; pZJM: NotI) and electroporated in 4 mm cuvettes (BioRad
93 GenePulser Xcell; exponential, 1.5kV, 25μF). Twenty-four h after electroporation, culture media
94 was supplemented with appropriate drug for selection: 15 μg/ml G418; 50 μg/ml hygromycin; 2.5
95 μg/ml phleomycin; 1 μg/ml puromycin; 10 μg/ml blasticidin. RNAi cell lines were generated by
96 nucleotides 41-441 of *Tb*Pex13.2 into the inducible pZJM vector possessing dual opposing T7
97 promoters and a phleomycin resistance marker (*19*). Usually we grow RNAi cell lines in tet-free
98 media to reduce leaky expression from RNAi plasmids. However, this was not required for these
99 cell lines as we did not observe leaky expression.

100

101 ***Tb*Pex13.2 antibody production:** Polyclonal guinea pig antisera was generated against
102 truncated recombinant *Tb*Pex13.2 (Thermo Scientific). Amino acids 2-150 of *Tb*Pex13.2 fused to
103 an N-terminal His_6 tag was expressed using the pQE30 expression system (Qiagen) and purified
104 using a Ni-NTA column under denaturing conditions using 8M urea as described (*20*).

105

106 **Growth curves**: Cells possessing the RNA inducible pZJM:*Tb*Pex13.2 vector were seeded at
107 10^5 cells/ml in SDM79 (PCF) or $5x10^4$ cells/ml HMI-9 (BSF) and induced with 1 μg/ml doxycycline.
108 PCF cells were allowed to grow to a density of $5x10^6$ cells/ml prior to passing back to $1x10^5$. BSF
109 cells were allowed to grow to a density of $1x10^6$ cells/ml prior to passing back to $5x10^4$ cells/ml.

110 Culture density was monitored by flow cytometry at 24 h intervals using an Accuri C6 flow
111 cytometer (BD Biosciences).
112
113 **Sucrose gradient fractionation and western blot:** Large-scale sucrose gradient fractionation
114 was carried out as described previously (*21*). Small-scale fractionations for *Tb*Pex13.2 silencing
115 were separated as described previously (*21*) with the following modifications: the post-nuclear
116 lysate was separated on a 13 ml 20%-40% linear Optiprep gradient at 170,000*g* for 19 h in a
117 Beckman SW-40Ti rotor at 4°C (acceleration 9 and deceleration coast), 500 µl fractions were
118 taken from the top of the gradient and the protein concentration was determined by BCA assay
119 (ThermoFisher). Protein from each fraction (2.5 µg) was separated by SDS-PAGE and analyzed
120 by western blotting with antibodies against the glycosomal proteins: *Tb*aldolase (1:20,000),
121 *Tb*Pex13.1 (1:10,000), *Tb*Pex13.2 (1:10,000), *Tb*Pex11 (1:4,000) provided by Dr. Christine
122 Clayton (Zentrum für Molekulare Biologie der Universität Heidelberg, Germany) (*22*), *Tb*PFK
123 (1:10,000) and *Tb*FBP (1:10,000) provided by Dr. Paul Michels (University of Edinburgh, UK), and
124 the ER protein *Tb*BiP (1:100,000) provided by Dr. Jay Bangs (University at Buffalo, Buffalo, NY)
125 (*18*).
126
127 **Protease protection assays**: Protease protection assays were carried out using a modified
128 protocol previously described (*22*). Cells (10^6) were harvested at 800*g* for 10 min, washed once
129 in PBS (150 mM NaCl, 1 mM KH_2PO_4, 5.6 mM Na_2HPO_4, pH 7.4), once in STE buffer (250 mM
130 sucrose, 25 mM Tris-HCl, pH7.4, 1 mM EDTA), and resuspended in 98 µl ice cold STEN buffer
131 (STE buffer supplemented with 150 mM NaCl) and 0.1 mM phenylmethylsulfonyl fluoride (PMSF).
132 Cells were permeabilized with 2 µl 1mg/ml digitonin (final concentration of 0.02 mg/ml), vortexed
133 for 5 sec and incubated at room temperature for 4 min. Following permeabilization, cells were
134 centrifuged at 20,000*g* for 2 min and resuspended in 85 µl STEN buffer. Pellets were treated
135 with either 10 µl water or Triton X-100 (1% v/v final) and either 5 µl water or 2 mg/ml proteinase

136 K. Reactions were incubated on ice for 30 min and stopped by addition of 10% w/v trichloroacetic
137 acid (TCA). Precipitated proteins were centrifuged at 17,000*g* for 10 min and washed once with
138 acetone before being resuspended in cracking buffer (CB; 10% glycerol, 2% SDS, 2% β-
139 mercaptoethanol, 100mM Tris, pH 6.8, 0.1% bromophenol blue) and boiled at 100°C. Proteins
140 were then analyzed by SDS-PAGE and western blotting.
141
142 **Membrane association assays:** Membrane association assays were carried out as previously
143 described by (*22*). For extraction of membrane proteins, 10^7 cells were centrifuged at 800*g* for
144 10 min and resuspended in 300 µl of ice-cold low-salt buffer for 15 min (5 mM Tris-HCl pH 7.8, 1
145 mM EDTA, 0.1 mM PMSF, 4 µg/ml leupeptin). Cells were then passed through a pipette tip 10x
146 and centrifuged at 20,000*g* for 30 min at 4°C. The insoluble pellet was resuspended in 300 µl
147 high-salt buffer (25 mM Tris-HCl pH7.8, 0.5 M KCl, 1 mM EDTA, 0.1 mM PMSF, 4 µg/ml leupeptin)
148 and incubated on ice for 15 min. After incubation, samples were centrifuged again at 20,000*g* for
149 30 min at 4°C. The insoluble pellet was resuspended in 300 µl 0.1 M Na_2CO_3 and incubated for
150 30 min on ice. Samples were then centrifuged at 120,000*g* for 1h at 4°C with a 500 µl cushion of
151 0.1 M Na_2CO_3, 0.25 M sucrose in a Beckman TLA100.3 rotor. Supernatant protein was
152 precipitated by 10% w/v TCA and washed once with acetone before being resuspended in CB.
153 Samples were then separated by SDS-PAGE and analyzed by western blot.
154

155 **Live cell microscopy:** Cells expressing either *Tb*AldoPTS2eYFP or *Tb*HKPTS2eYFP (Fig. 6B)
156 were washed once with PBS, mounted on a slide and visualized using a Zeiss Axiovert 200M
157 inverted fluorescence microscope with a 100x objective (N.A. 1.3). Images were analyzed using
158 AxioVision software version 4.8.2.
159

160 **Immunofluorescence microscopy:** All steps were performed at room temperature. Cells were
161 harvested (800*g*, 10 min), washed once with PBS, fixed with 2% paraformaldehyde in PBS for 30
162 min and allowed to settle on slides for 30 min. Adhered cells were washed once with wash
163 solution (0.1% normal goat serum in PBS) and permeabilized with 0.5% Trition X-100 for 30 min.
164 Following permeabilization, cells were washed twice with wash solution and blocked with 10%
165 normal goat serum (NGS) in PBS with 0.1% Triton X-100. Primary antibodies were diluted in
166 block solution (C-myc, Thermo Fisher 9E10 1:500; *Tb*Aldolase 1:500; *Tb*HK 1:500; *Tb*FBP
167 1:1,000; *Tb*PFK 1:500) and incubated with cells for 1 h. Following primary antibody, slides were
168 washed 3x with wash solution and incubated 1 h with secondary antibody (goat anti-mouse Alexa
169 fluor 488 1:1,000, goat anti-rabbit Alexa fluor 568 or Alexa fluor 647 1:1,000); (Thermo fisher) in
170 block. Wide-field images were taken using a Zeiss Axiovert 200M, 100x objective (N.A. 1.3), and
171 analyzed using AxioVision software version 4.8.2. Super-resolution images were obtained using
172 a Leica SP8X microscope equipped with HyD detector and 63x objective (N.A. 1.4).
173
174 **Electron microscopy processing and imaging**: Cells were harvested ($5x10^7$, 800*g* 10 min),
175 washed three times with PBS, and fixed (2% paraformaldehyde, 2.5% glutaraldehyde in 100mM
176 phosphate buffer pH 7.4). Cells were stored at 4°C for no longer than 2 days before being
177 processed as described previously (*23*). Glycosome area measurements were performed using
178 FIJI. Area of visible glycosomes for 15 fields was measured using the measure tool. To calculate
179 the glycosome area as a percentage of cell area, the area of glycosomes from each cell was
180 summed and divided by the total cell area visible.

181 **Biochemical analysis of glycosome protein localization**: Cells were seeded at $1x10^5$ cells/ml
182 and RNAi against *Tb*Pex13.2 was induced with 1 µg/ml doxycycline. After 4 days of induction,
183 cells were harvested (800*g*, 10 min) and washed once with PBS. Cells ($2x10^7$) were lysed using
184 1 volume wet weight silicon carbide abrasive and breakage confirmed by microscopy. Abrasive

185 was removed by centrifugation (100*g*, 1 min) and supernatant was transferred to a new tube,
186 followed by removal of nuclei (1,000*g*, 15 min). Supernatant was transferred to a new tube and
187 the organelle-rich fraction was separated from the cytosolic fraction by centrifugation (17,000*g*,
188 15 min). Cytosolic proteins were precipitated with 4 volumes of acetone, incubated on ice for 1
189 h, and centrifuged at 17,000*g* for 10 min, 4°C. Pelleted organelle-rich fraction and cytosolic
190 proteins were separated by SDS-PAGE and proteins detected by western blotting.
191
192 **RESULTS**
193
194 ***Tb*Pex13.2 is expressed in BSF and PCF parasites**
195 Antibodies raised against recombinant *Tb*Pex13.2 detected a protein of the expected size (~ 28
196 KDa) in PCF and BSF parasites, which was reduced upon induction of RNA interference (Fig. 1).
197 These antibodies sometimes detected a larger ~50 kDa protein. This larger band was not reduced
198 in *Tb*Pex13.2 RNAi cell lines, suggesting it was a non-specific, cross-reactive protein. To confirm
199 that this upper band was not a dimer of *Tb*Pex13.2, we treated lysates with DTT (10 mM) and
200 NEM (10 mM) to block free reactive thiols and prevent dimerization post-lysis. Neither treatment
201 affected the abundance of the 50 kDa species (Fig. S1).
202
203 ***Tb*Pex13.2 is an integral glycosomal membrane protein with its N-terminus exposed to the**
204 **cytosol**
205 To confirm that *Tb*Pex13.2 was localized to glycosomes, we resolved organelles via density
206 gradients and analyzed fractions by western blotting with antibodies against *Tb*BiP and
207 *Tb*aldolase. Under our conditions, the ER is less dense than glycosomes and equilibrates at the
208 top of the gradient. Consistent with being a glycosome protein, *Tb*Pex13.2 was detected in
209 fractions 14-20 that also contained the glycosome protein aldolase (Fig. 2). In contrast, the ER
210 protein, *Tb*BiP, was detected in fractions 20-32.

211

212 *Tb*Pex13.2 is predicted to have at least 2 transmembrane (TM) domains (*14*, *24*). To confirm that
213 *Tb*Pex13.2 is an integral membrane protein, we sequentially extracted membrane-enriched
214 fractions with low-salt, high-salt, and sodium carbonate (Fig. 3A). The soluble glycosome matrix
215 protein *Tb*aldolase was detected in the low and high-salt supernatants, whereas *Tb*Pex13.2 was
216 detected only in the pellet following sodium carbonate extraction, as expected for an integral
217 membrane protein. Orientation of the protein in the membrane was determined by protease
218 protection assays with cells expressing *Tb*Pex13.2 fused to either an N-terminal myc epitope
219 (myc*Tb*Pex13.2) or an N-terminal mycBirA* tag (mycBirA**Tb*Pex13.2). Treatment of cells with
220 proteinase K (PK) in the absence of Triton X-100 resulted in loss of myc signal, indicating that the
221 N-terminus of the protein was accessible by PK and exposed to the cytosol (Fig. 3B). *Tb*aldolase
222 is a matrix protein with a protease resistant core. Full-length *Tb*aldolase is detected in PK
223 treatment without detergent indicating that glycosome integrity is not compromised during
224 treatment. After treatment with PK and detergent, we observed a smaller proteolytic product as
225 seen in previous studies documenting the protease-resistant nature of *Tb*aldolase (*25*). These
226 results suggest that the N-terminus of *Tb*Pex13.2 is on the cytosolic side of the glycosome
227 membrane.

228

229 ***Tb*Pex13.2 is localized to discrete foci in glycosomes**

230 Antibodies raised against recombinant *Tb*Pex13.2 do not work in immunofluorescence assays
231 (IFA). Because of this, we analyzed cell lines expressing *Tb*Pex13.2 fused to an N-terminal myc
232 tag (myc*Tb*Pex13.2) (Fig. 4 A, B). Anti-myc antibodies labeled punctate structures that were
233 distributed throughout the cell and exhibited limited overlap with the glycosome marker
234 *Tb*aldolase. We used Mander's overlap coefficients (MOCs) to quantify the extent to which
235 myc*Tb*Pex13.2 co-localized with the glycosome marker aldolase and the ER marker *Tb*BiP (Fig.
236 4 C, D). MOC values range from 0 (no overlap) to 1 (complete overlap) (*26*). MOC for *Tb*aldolase

237 and myc*Tb*Pex13.2 was 0.62 ± 0.16 suggesting limited co-localization. To better define the
238 relationship between myc*Tb*Pex13.2 and *Tb*aldolase staining, we calculated Mander's M1 and
239 M2 values, which reveal the extent to which pixels in one channel overlap with the other. The M1
240 and M2 values were 0.49 ± 0.20 and 0.91 ± 0.10, respectively. These numbers indicate that 49%
241 of the signal in channel 1 (*Tb*aldolase) overlaps with channel 2 (myc) and that 91% of the signal
242 in channel 2 (myc) overlaps with channel 1 (*Tb*aldolase). These results suggest that
243 myc*Tb*Pex13.2 is limited to a restricted portion of the glycosome. MOC values for *Tb*BiP and
244 myc*Tb*Pex13.2 was 0.17 ± 0.07, suggesting that these two proteins do not co-localize. In
245 agreement with the MOC, M1 and M2 values, we observed that myc*Tb*Pex13.2 was not evenly
246 distributed throughout glycosomes but was restricted to a few distinct foci within each organelle.
247 Thirty-seven percent of the myc*Tb*Pex13.2-positive glycosomes had one foci, 35% had two foci,
248 and 24% had 3 or more. Of *Tb*aldolase positive glycosomes, approximately 4% had no visible
249 myc*Tb*Pex13.2 foci (Fig. 4E).
250
251 **Silencing of *Tb*Pex13.2 in PCF parasites reduced import efficiency of PTS2 proteins**
252 Prior work revealed that silencing *Tb*Pex13.2 in BSF parasites was detrimental (*14*). At that time
253 PCF RNAi cell lines could not be established. We were able to silence *Tb*Pex13.2 in both PCF
254 and BSF parasites via inducible RNA interference and western analysis indicated that *Tb*Pex13.2
255 levels were reduced ~95% upon induction of RNAi (Fig. 1). Silencing of *Tb*Pex13.2 did not alter
256 the overall expression levels of the glycosome matrix protein *Tb*aldolase, or the glycosome
257 membrane proteins *Tb*Pex13.1 or *Tb*Pex14 (Fig. 5A) in BSF or PCF parasites. While we observed
258 no change in growth rate after induction of RNAi in PCF parasites (Fig. 5B), BSF growth was
259 slowed upon induction of silencing (Fig. 5C) as reported previously (*14*).
260
261 In higher eukaryotes, Pex13 functions in peroxisomal protein import. We used
262 immunofluorescence assays (IFA) to determine if *Tb*Pex13.2 silencing altered glycosome protein

263 import in PF parasites. In uninduced cells, the glycosome proteins *Tb*aldolase, *Tb*HK, *Tb*FBP
264 and *Tb*PFK all localized to punctate structures characteristic of glycosomes (Fig. 6A). After 4
265 days of induction, IFA revealed an increase in the cytosolic localization of *Tb*aldolase. In contrast,
266 the localization of *Tb*HK, *Tb*FBP, and *Tb*PFK was not altered in these cells. Under standard
267 culturing conditions in SDM79 media (5 mM glucose), the mislocalization of glycosome proteins
268 is generally lethal. Previous work has shown that removal of glucose from the media rescues this
269 phenotype (*27*). We measured glycosome protein localization in low-glucose media (SDM79θ, 5
270 μM glucose) with the expectation that under these conditions we could score phenotypes that
271 would be lethal in cells grown in SDM79. When cells were grown in SDM79θ, tet-induced
272 mislocalization of *Tb*aldolase was increased. In contrast, even in low-glucose conditions, the
273 *Tb*HK, *Tb*FBP and *Tb*PFK localization was not altered upon TbPex13.2 silencing.
274
275 To quantify import efficiencies of each protein, we used western analysis to determine the percent
276 of protein associated with organelle fractions in uninduced and induced *Tb*Pex13.2 RNAi cell
277 lines. Cells were lysed and centrifuged to obtain a membrane-rich fraction and western analysis
278 used to calculate the percentage of each protein associated with membrane (glycosomes) and
279 soluble (cytosolic) fractions (Fig. 6C). In uninduced cells, 58 ± 5% of *Tb*aldolase was associated
280 with the pellet compared to 48.5 ± 5% in induced cells. This mislocalization was increased in low-
281 glucose media with 58.5 ± 5% associated with the pellet in uninduced cells and 38 ± 4% in
282 *Tb*Pex13.2 silenced cells. In contrast, *Tb*aldolase, *Tb*FBP, *Tb*PFK, and *Tb*HK localization did not
283 change significantly when *Tb*Pex13.2 was silenced in high or low-glucose media. While both
284 *Tb*HK and *Tb*aldolase have type 2 peroxisomal targeting sequences (PTS2s), only *Tb*aldolase
285 localization was affected by *Tb*Pex13.2 silencing. To assess the extent to which each PTS2
286 sequence contributed to this *Tb*Pex13.2-dependent localization, we followed the localization of
287 eYFP fused to either the PTS2 of *Tb*aldolase or *Tb*HK. Fluorescence microscopy of living cells

288 revealed that both *Tb*AldoPTS2eYFP and *Tb*HKPTS2eYFP were mislocalized to the cytoplasm
289 in TbPex13.2 deficient cells (Fig. 6B).
290
291 We next used transmission electron microscopy (TEM) to determine how depletion of *Tb*Pex13.2
292 altered overall glycosome morphology (Fig. 7A). Under these conditions, glycosomes are
293 spherical, electron dense organelles. In SDM79 media, glycosomes comprised 3.67% ± 1.76%
294 and 2.14% ± 0.84% of the cell volume in wild-type or *Tb*Pex13.2-deficient cells, respectively. In
295 SDM79θ media, glycosomes comprised 6.18% ± 1.75% and 5.77% ± 2.11% of the cell volume in
296 wild-type or *Tb*Pex13.2-deficient cells, respectively. These results suggest that glycosomes
297 morphology was not dramatically altered upon reduction of *Tb*Pex13.2 levels.
298
299 We reasoned that *Tb*Pex13.2 silencing may interfere with the import of proteins for which we have
300 no antibodies. Additionally, depletion of a protein localized to the glycosome membrane may
301 affect other biochemical properties such as density. To assess this, we resolved organelles on a
302 sucrose/Optiprep gradient and followed sedimentation via western analysis of glycosomal
303 proteins. In uninduced cells, *Tb*aldolase and *Tb*Pex14 were detected in fractions 10-16 as is
304 typical for glycosome proteins. In induced cells, however, these proteins were detected in higher
305 fractions (4-16) suggesting that glycosomes in *Tb*Pex13.2 deficient cells are lighter than those
306 isolated from parental cells. In contrast, western analysis with anti-*Tb*BiP antibodies revealed
307 that the sedimentation of the ER was not altered in *Tb*Pex13.2 deficient cells.
308
309 **DISCUSSION**
310 Kinetoplastids harbor specialized peroxisomes called glycosomes that are essential to parasite
311 survival. The majority of the glycolytic pathway is compartmentalized within these organelles and
312 disruption of compartmentalization is lethal under standard conditions (*5*, *8*, *27–29*). As

313 glycosomes are essential organelles in kinetoplastids, the mechanisms for their maintenance are
314 attractive drug targets (*4*, *30*, *31*).
315
316 Like peroxisomes, glycosomes do not have DNA and all matrix proteins are imported post-
317 translationally in a process that is fairly well-conserved. Glycosome and peroxisome matrix
318 proteins are synthesized in the cytoplasm where they are identified by the soluble receptors, Pex5
319 and Pex7, which recognize peroxisomal targeting sequence (PTS) 1 and PTS2, respectively (*8*).
320 The receptor:cargo complex is then targeted to the receptor docking complex on the
321 glycosome/peroxisome membrane containing the proteins Pex13 and Pex14 (*7*, *12*, *32*). *T.*
322 *brucei* is unusual in that it has two Pex13s, which have been named *Tb*Pex13.1 and *Tb*Pex13.2
323 (*14*, *15*). The two proteins share low overall sequence identity with each other or with other
324 Pex13s. *Tb*Pex13.1 was the first to be identified in *T. brucei.* Fusions with green fluorescent
325 protein localized to glycosomes and silencing *Tb*Pex13.1 resulted in glycosome protein
326 mislocalization and cell death. *Tb*Pex13.2 was identified later and silencing of this protein in BSF
327 parasites resulted in glycosome protein mislocalization and cell death. These findings indicate
328 that the two proteins are not redundant, however, the specific role that each plays in glycosome
329 biogenesis is unclear.
330
331 Here, we report the characterization of *Tb*Pex13.2 and a phenotypic characterization of RNA
332 interference cell lines in which *Tb*Pex13.2 is silenced. In agreement with previous work, we found
333 that silencing *Tb*Pex13.2 slowed the growth rate of BSF parasites (*14*). While the effect we
334 observed was not as dramatic as previous work, this is likely due to variation in penetrance. As
335 previously observed with the tagged *Tb*Pex13.2 (*14*), we found that native *Tb*Pex13.2 was an
336 integral glycosome membrane protein. Furthermore, we were able to demonstrate through
337 protease protection assays that the N-terminus of *Tb*Pex13.2 is exposed to the cytosol where it
338 can interact with proteins involved in protein import. Unfortunately, we could not express C-

339 terminally tagged *Tb*Pex13.2 in *T. brucei* and were not able to determine if the C-terminus is
340 localized to the cytosolic or matrix side of the glycosome.
341
342 We found that *Tb*aldolase, which has a PTS2 sequence was mislocalized in *Tb*Pex13.2-deficient
343 parasites while the import of PFK harboring a PTS1 was not affected. During the import process,
344 Pex7 binds to the N-terminus of Pex13 that is comprised of a YG rich sequence in *S. cerevisiae*
345 and *A. thaliana* (*33*, *34*). Both *Tb*Pex13.1 and *Tb*Pex13.2 have a similar YG rich domain in their
346 N-termini. It may be that depletion of *Tb*Pex13.2 reduces the number of Pex7 binding sites at the
347 glycosome membrane resulting in reduced PTS2 import while having minimal effect on protein
348 import of PTS1 proteins such as PFK. *Tb*FBP import was not affected in *Tb*Pex13.2-deficient
349 cells, however, this protein has both PTS1 and PTS2 sequences and may be imported by a
350 combination of PTS1 *and* PTS2 import pathways.
351
352 In previous studies using BSF parasites, digitonin extractions revealed that silencing *Tb*Pex13.2
353 impaired import of both PTS1 and PTS2 proteins. So far, we have not observed defects in PCF
354 PTS1 import. This may be because we followed the import of a different set of proteins due to
355 antibody availability. Additionally, it may be that the role of *Tb*Pex13.2 in protein import varies
356 with lifecycle stage. Finally, the observed differences may be a consequence of the methods
357 used to assess import. Previous studies utilized digitonin fractionations while we measured import
358 via IFA and quantification of organelle associated proteins.
359
360 The selective defect in aldolase (PTS2) protein import may be a reflection of the different
361 mechanisms that direct PTS2 and PTS1 protein import. The receptor Pex7, unlike Pex5, is
362 necessary but not sufficient for PTS2 protein import and several PTS2 co-receptors have been
363 described. These co-receptors are species-specific and include Pex18 and Pex21p in
364 *Saccharomyces cerevisiae* (*35*), Pex20p in *Yarrowia lipolytica* (*36*), and the long isoform of Pex5

365 (Pex5L) in mammals (*37*). All three co-receptors have Pex7-binding domains. *T. brucei* has two
366 isoforms of Pex5, however, the functional significance of the two forms are very different from
367 what is observed in mammals. Whereas, *Hs*Pex5L is a splicing variant with an internal Pex7BD,
368 *Tb*Pex5L is the full-length protein while the shorter form is a result of a proteolytic cleavage (*38*).
369 Therefore, a co-receptor has not yet been identified in *T. brucei*. It is attractive to speculate that
370 *Tb*Pex13.2 may be playing this role in kinetoplastids. Indeed, the N-terminus containing the YG-
371 rich region faces the cytoplasm and is physically positioned to function in this capacity.
372
373 We were surprised to find that *Tb*aldolase and *Tb*HK, which both have PTS2s, behaved differently
374 in *Tb*Pex13.2 deficient cells. *Tb*aldolase import was disrupted while *Tb*HK was not. We imagine
375 two possible scenarios for these results. It is possible that not all PTS2s are with the same
376 efficiency. Alternatively, there may be information outside of the PTS2 sequence that influences
377 the glycosome localization of *Tb*HK. To discern which scenario was at play, we fused the PTS2
378 of *Tb*HK and the PTS2 of *Tb*aldolase to enhanced yellow fluorescent protein (eYFP) and found
379 that the import of each is disrupted in *Tb*Pex13.2-deficient cells. This finding indicates *Tb*Pex13.2
380 is required for efficient import of both PTSs and reveals that that *Tb*HK contains information for
381 glycosomal localization outside of the PTS2 sequence.
382
383 The formation of myc*Tb*Pex13.2 foci on the glycosome membrane was interesting because of its
384 similarity to the localization of other import process-related peroxins in other systems. Recent
385 super-resolution studies of peroxisomes have provided insight into the heterogeneous distribution
386 of different peroxins within peroxisomes (*39*). Membrane-bound Pex5 and Pex14 generally
387 colocalized in structures that range in shape from round to elliptical, ring-like structures. Pex11,
388 which functions in peroxisome proliferation and not protein import, and a soluble matrix protein
389 SCP2 also exhibit heterogenous distribution. The functional relevance of these distribution
390 patterns is unclear; however, the use of super-resolution imaging is essential to resolving the

391 mechanism and consequence of such localization patterns. To our knowledge, this is the only
392 example of heterogenous intra-glycosomal localization of peroxins in parasites and future studies
393 are necessary to understand the significance of such localizations.
394
395 **Acknowledgements**
396 This work was funded by an NSF COBRE P20 grant P20GM109094. We thank Clemson Light
397 Imaging Facility for imaging assistance and use of equipment and Dr. Jay Bangs (University of
398 Buffalo, Buffalo, NY), Dr. Christine Clayton (Zentrum für Molekulare Biologie der Universität
399 Heidelberg, Germany), and Dr. Paul Michels (University of Edinburgh, UK) for antibodies. We
400 also thank Wandy Beatty (Washington University in St. Louis) for contributing to the transmission
401 electron microscopy work.
402
403

404 **Figure Legends**

405

406 **Figure 1. Antibodies raised against recombinant *Tb*Pex13.2 recognize a 28 kDa protein in**
407 **PCF and BSF parasites that is reduced upon induction of RNAi.** PCF and BSF parasites
408 harboring pZJM:*Tb*Pex13.2 were grown for 4 days with and without doxycycline to induce RNAi.
409 Lysates from $2x10^6$ cells were probed with antisera generated against r*Tb*Pex13.2 aa2-150.
410 Tubulin was used as a loading control. *Larger cross-reactive band.

411

412 **Figure 2. *Tb*Pex13.2 equilibrates with glycosome proteins in density gradients.** Post-
413 nuclear cell lysate was centrifuged through an Optiprep/sucrose gradient and 1ml fractions were
414 collected from the bottom of the gradient. Protein was precipitated, separated by SDS-PAGE,
415 and analyzed by western blot with antibodies against *Tb*aldolase, *Tb*BiP, and *Tb*Pex13.2.

416

417 **Figure 3. *Tb*Pex13.2 is an integral membrane protein with the N-terminus exposed to the**
418 **cytosol.** (A) Membrane protein extraction of whole cell membranes. Cells (10^7) were
419 sequentially extracted with low-salt, high-salt, and sodium carbonate. Proteins were
420 precipitated from supernatants (LS, HS, CS) and final carbonate pellet (CP), separated by SDS-
421 PAGE, transferred to nitrocellulose, and analyzed by western blotting with antibodies against
422 *Tb*Pex13.2 and aldolase. (B) Protease protection assay. Cell lysate (lane 1) were treated with
423 Triton X-100 (lane 2), protease K (lane 3), or Triton X-100 and protease K (lane 4). Samples
424 were resolved by SDS-PAGE and analyzed by western blots with anti-myc antibodies.

425

426 **Figure 4. Epitope-tagged myc*Tb*Pex13.2 localizes to glycosomes.** (A,B) Cells were fixed,
427 permeabilized, and stained with antibodies against myc (green) and *Tb*aldolase or *Tb*BiP
428 (magenta). Representative images of maximum intensity projections of deconvolved Z-stacks
429 are shown. Scale bar indicates 5 μm. (C) Plots of Mander's overlap coefficients (MOC) and

430 Manders M1 and M2 values were calculated from individual cells using Z-stacks with the Mander's
431 coefficient plugin in FIJI. Each point represents analysis of one cell. Myc*Tb*Pex13.2 and
432 *Tb*Aldolase n=34. myc*Tb*Pex13.2 and *Tb*BiP n=27. (D) MOC, M1 and M2 values. (E) Pie chart
433 representing the counted number of myc*Tb*Pex13.2 foci per organelle.
434
435 **Figure 5. Silencing of *Tb*Pex13.2 does not influence expression of other glycosome**
436 **proteins and slows BSF growth.** (A) Cultures were grown for 96 h and $5x10^6$ cells were
437 analyzed by western blotting with antibodies against *Tb*Pex13.2, *Tb*Pex13.1, *Tb*aldolase, and
438 *Tb*Pex14. Tubulin was used as a loading control. Growth curves for PCF (B) and BSF (B)
439 parasites grown with and without doxycycline.
440
441 **Figure 6. Silencing of *Tb*Pex13.2 results in mislocalization of a subset of glycosome**
442 **proteins.** (A) IFA assays of PCF cells grown in the presence or absence of doxycycline (DOX).
443 Cells were labeled with antibodies against *Tb*aldolase, *Tb*hexokinase, and *Tb*fructose 1,6-
444 bisphosphatase (*Tb*FBP) and detected using goat anti-rabbit secondary antibodies conjugated
445 with Alexa Fluor 488 (Green). Nuclear and kinetoplast DNA were stained with DAPI (Blue). (B)
446 Live cell microscopy of cells constitutively expressing eYFP fused with the peroxisome targeting
447 sequence 2 (PTS2) of aldolase or hexokinase (Green). (C) Biochemical analysis of
448 mislocalization. Cells were lysed by silicon carbide abrasive and were centrifuged to obtain an
449 organelle enriched pellet. Cytosol proteins in supernatant were precipitated using 4 volumes of
450 acetone. Samples were separated by SDS-PAGE and analyzed by western blot. Mislocalization
451 was quantified by densitometry of three biological replicates using ImageJ.
452
453 **Figure 7. Electron microscopy of *Tb*Pex13.2 deficient cells.** (A) EM analysis of wildtype and
454 cells induced for RNAi (B) Analysis of glycosome size and area as a percentage of cell area.
455 Twenty-five fields and at least 36 glycosomes per condition were measured.

456

457 **Figure 8. Glycosomes from *Tb*Pex13.2-deficient cells are lighter than wild-type.** (A) Cells
458 ($5x10^8$) were harvested, lysed mechanically with silicon carbide, and the glycosome-enriched
459 pellet resolved on a linear Optiprep gradient. Fractions were taken from the top of the gradient
460 and analyzed by western blotting. Boxes indicate glycosome fractions (B) Western blot bands
461 were quantified using densitometry and the percentage of protein in each fraction was plotted.
462 Presented is a representative gel from three biological replicates.

463

464 **Figure S1. Higher molecular weight bands are not multimers of *Tb*Pex13.2.** Bloodstream
465 form (10^6) lysates were treated with DTT to reduce disulfide bonds and NEM to block free
466 reactive thiols to prevent dimerization post lysis. Lysates were resolved by SDS-PAGE and
467 western blots probed with α-*Tb*Pex13.2 antibodies. Asterisk indicates non-specific cross-
468 reactive band.

469 **References**

470 1. T. Gabaldón, M. L. Ginger, P. A. M. Michels, Peroxisomes in parasitic protists. *Mol.*
471 *Biochem. Parasitol.* (2016), doi:10.1016/j.molbiopara.2016.02.005.
472 2. M. Parsons, T. Furuya, S. Pal, P. Kessler, Biogenesis and function of peroxisomes and
473 glycosomes. *Mol. Biochem. Parasitol.* **115**, 19–28 (2001).
474 3. J. Moyersoen, J. Choe, E. Fan, W. G. J. Hol, P. a M. Michels, Biogenesis of peroxisomes
475 and glycosomes: Trypanosomatid glycosome assembly is a promising new drug target.
476 *FEMS Microbiol. Rev.* **28**, 603–643 (2004).
477 4. J. R. Haanstra *et al.*, Compartmentation prevents a lethal turbo-explosion of glycolysis in
478 trypanosomes. *Proc. Natl. Acad. Sci. U. S. A.* **105**, 17718–23 (2008).
479 5. C. Guerra-Giraldez, L. Quijada, C. E. Clayton, Compartmentation of enzymes in a
480 microbody, the glycosome, is essential in Trypanosoma brucei. *J. Cell Sci.* **115**, 2651–
481 2658 (2002).
482 6. V. C. Kalel *et al.*, Inhibitors of glycosomal protein import provide new leads against
483 trypanosomiasis. *Microb. cell (Graz, Austria)*. **4**, 229–232 (2017).
484 7. J. J. Smith, J. D. Aitchison, Peroxisomes take shape. *Nat. Rev. Mol. Cell Biol.* **14**, 803–17
485 (2013).
486 8. N. Galland *et al.*, Characterization of the role of the receptors PEX5 and PEX7 in the
487 import of proteins into glycosomes of Trypanosoma brucei. *Biochim. Biophys. Acta - Mol.*
488 *Cell Res.* **1773**, 521–535 (2007).
489 9. P. K. Kim, E. H. Hettema, Multiple pathways for protein transport to peroxisomes. *J. Mol.*
490 *Biol.* **427**, 1176–1190 (2015).
491 10. S. J. Gould, G. A. Keller, N. Hosken, J. Wilkinson, S. Subramani, A conserved tripeptide
492 sorts proteins to peroxisomes. *J. Cell Biol.* **108**, 1657–1664 (1989).
493 11. P. Rehling *et al.*, The import receptor for the peroxisomal targeting signal 2 (PTS2) in
494 Saccharomyces cerevisiae is encoded by the PAS7 gene. *EMBO J.* **15**, 2901–13 (1996).

495 12. C. Williams, B. Distel, Pex13p: Docking or cargo handling protein? *Biochim. Biophys.*
496 *Acta - Mol. Cell Res.* **1763**, 1585–1591 (2006).
497 13. T. Saveria, P. Kessler, B. C. Jensen, M. Parsons, Characterization of glycosomal RING
498 finger proteins of trypanosomatids. *Exp. Parasitol.* **116**, 14–24 (2007).
499 14. A. Brennand, D. J. Rigden, P. A. M. Michels, Trypanosomes contain two highly different
500 isoforms of peroxin PEX13 involved in glycosome biogenesis. *FEBS Lett.* **586**, 1765–
501 1771 (2012).
502 15. E. Verplaetse, D. J. Rigden, P. A. M. Michels, Identification, characterization and
503 essentiality of the unusual peroxin 13 from Trypanosoma brucei. *Biochim. Biophys. Acta -*
504 *Mol. Cell Res.* **1793**, 516–527 (2009).
505 16. E. Wirtz, C. Clayton, Inducible gene expression in trypanosomes mediated by a
506 prokaryotic repressor. *Science*. **268**, 1179–83 (1995).
507 17. Y. Qiu *et al.*, Glucose Signaling Is Important for Nutrient Adaptation during Differentiation
508 of Pleomorphic African Trypanosomes (2018), doi:10.1128/mSphere.00366-18.
509 18. J. D. Bangs, E. M. Brouch, D. M. Ransom, J. L. Roggy, A soluble secretory reporter
510 system in Trypanosoma brucei. Studies on endoplasmic reticulum targeting. *J. Biol.*
511 *Chem.* **271**, 18387–18393 (1996).
512 19. Z. Wang, J. C. Morris, M. E. Drew, P. T. Englund, Inhibition of Trypanosoma brucei gene
513 expression by RNA interference using an integratable vector with opposing T7 promoters.
514 *J. Biol. Chem.* **275**, 40174–40179 (2000).
515 20. QIAGEN, *The QIA expressionist ™-His tag proteins* (2003).
516 21. C. Colasante, M. Ellis, T. Ruppert, F. Voncken, Comparative proteomics of glycosomes
517 from bloodstream form and procyclic culture form Trypanosoma brucei brucei.
518 *Proteomics*. **6**, 3275–3293 (2006).
519 22. P. Lorenz, A. G. Maier, E. Baumgart, R. Erdmann, C. Clayton, Elongation and clustering
520 of glycosomes in Trypanosoma brucei overexpressing the glycosomal Pex11p. *EMBO J.*

521 **17**, 3542–3555 (1998).
522 23. S. Bauer, J. C. Morris, M. T. Morris, Environmentally regulated glycosome protein
523 composition in the African trypanosome. *Eukaryot. Cell*. **12**, 1072–1079 (2013).
524 24. A. Krogh, B. Larsson, G. Von Heijne, E. L. L. Sonnhammer, Predicting transmembrane
525 protein topology with a hidden Markov model: Application to complete genomes. *J. Mol.*
526 *Biol.* **305**, 567–580 (2001).
527 25. C. E. Clayton, Import of fructose bisphosphate aldolase into the glycosomes of
528 Trypanosoma brucei. *J. Cell Biol.* **105**, 2649–2654 (1987).
529 26. V. Zinchuk, O. Zinchuk, T. Okada, Quantitative Colocalization Analysis of Multicolor
530 Confocal Immunofluorescence Microscopy Images: Pushing Pixels to Explore Biological
531 Phenomena. *Acta Histochem. Cytochem.* **40**, 101–111 (2007).
532 27. T. Furuya *et al.*, Glucose is toxic to glycosome-deficient trypanosomes. *Proc. Natl. Acad.*
533 *Sci. U. S. A.* **99**, 14177–14182 (2002).
534 28. S. K. Banerjee, P. S. Kessler, T. Saveria, M. Parsons, Identification of trypanosomatid
535 PEX19: Functional characterization reveals impact on cell growth and glycosome size
536 and number. *Mol. Biochem. Parasitol.* **142**, 47–55 (2005).
537 29. V. C. Kalel, W. Schliebs, R. Erdmann, Identification and functional characterization of
538 Trypanosoma brucei peroxin 16. *Biochim. Biophys. Acta - Mol. Cell Res.* (2015),
539 doi:10.1016/j.bbamcr.2015.05.024.
540 30. P. a M. Michels, F. Bringaud, M. Herman, V. Hannaert, Metabolic functions of
541 glycosomes in trypanosomatids. *Biochim. Biophys. Acta - Mol. Cell Res.* **1763**, 1463–
542 1477 (2006).
543 31. M. Parsons, Glycosomes: Parasites and the divergence of peroxisomal purpose. *Mol.*
544 *Microbiol.* **53**, 717–724 (2004).
545 32. A. Schell-Steven *et al.*, Identification of a novel, intraperoxisomal pex14-binding site in
546 pex13: association of pex13 with the docking complex is essential for peroxisomal matrix

547 protein import. *Mol. Cell. Biol.* **25**, 3007–3018 (2005).
548 33. K. Stein, A. Schell-Steven, R. Erdmann, H. Rottensteiner, Interactions of Pex7p and
549 Pex18p/Pex21p with the peroxisomal docking machinery: implications for the first steps in
550 PTS2 protein import. *Mol. Cell. Biol.* **22**, 6056–69 (2002).
551 34. S. Mano, C. Nakamori, K. Nito, M. Kondo, M. Nishimura, The Arabidopsis *pex12* and
552 *pex13* mutants are defective in both PTS1- and PTS2-dependent protein transport to
553 peroxisomes. *Plant J.* **47**, 604–618 (2006).
554 35. P. E. Purdue, X. Yang, P. B. Lazarow, Pex18p and Pex21p, a novel pair of related
555 peroxins essential for peroxisomal targeting by the PTS2 pathway. *J. Cell Biol.* **143**,
556 1859–1869 (1998).
557 36. V. I. Titorenko, J. J. Smith, R. K. Szilard, R. A. Rachubinski, Pex20p of the yeast
558 Yarrowia lipolytica is required for the oligomerization of thiolase in the cytosol and for its
559 targeting to the peroxisome. *J. Cell Biol.* **142**, 403–20 (1998).
560 37. M. Kunze *et al.*, Mechanistic insights into PTS2-mediated peroxisomal protein import: the
561 co-receptor PEX5L drastically increases the interaction strength between the cargo
562 protein and the receptor PEX7. *J. Biol. Chem.* **290**, 4928–40 (2015).
563 38. M. Gualdrón-López, P. A. M. Michels, Processing of the glycosomal matrix-protein import
564 receptor PEX5 of Trypanosoma brucei. *Biochem. Biophys. Res. Commun.* **431**, 98–103
565 (2013).
566 39. S. Galiani *et al.*, Super-resolution microscopy reveals compartmentalization of
567 peroxisomal membrane proteins. *J. Biol. Chem.* **291**, 16948–16962 (2016).
568

Figure 1

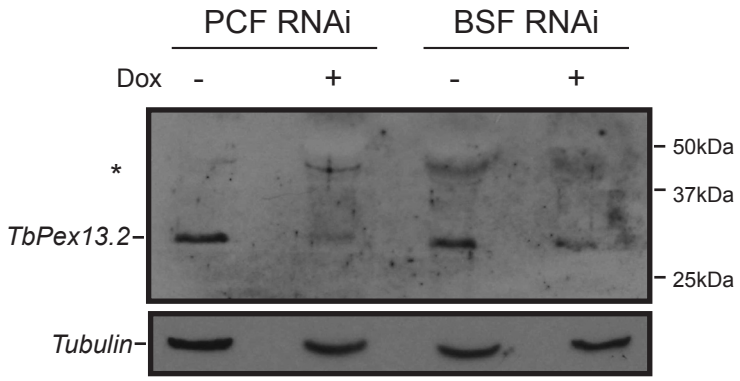

Figure 2

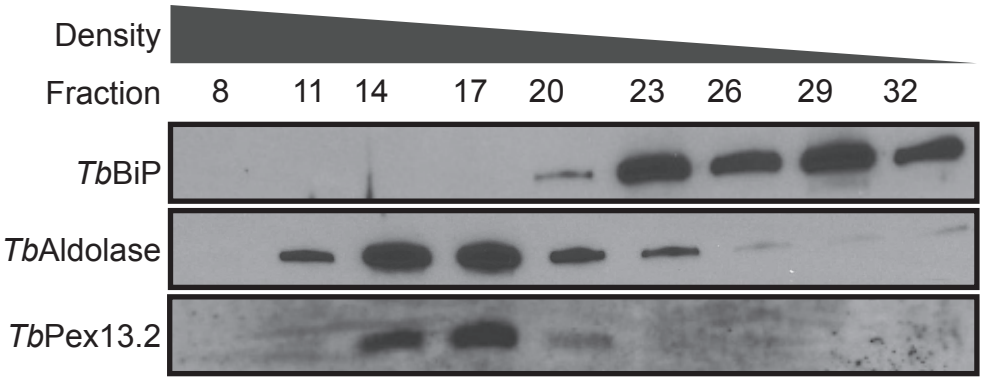
Density
Fraction
8
11
14
17
20
23
26
29
32
*Tb*BiP
*Tb*Aldolase
*Tb*Pex13.2

Figure 3

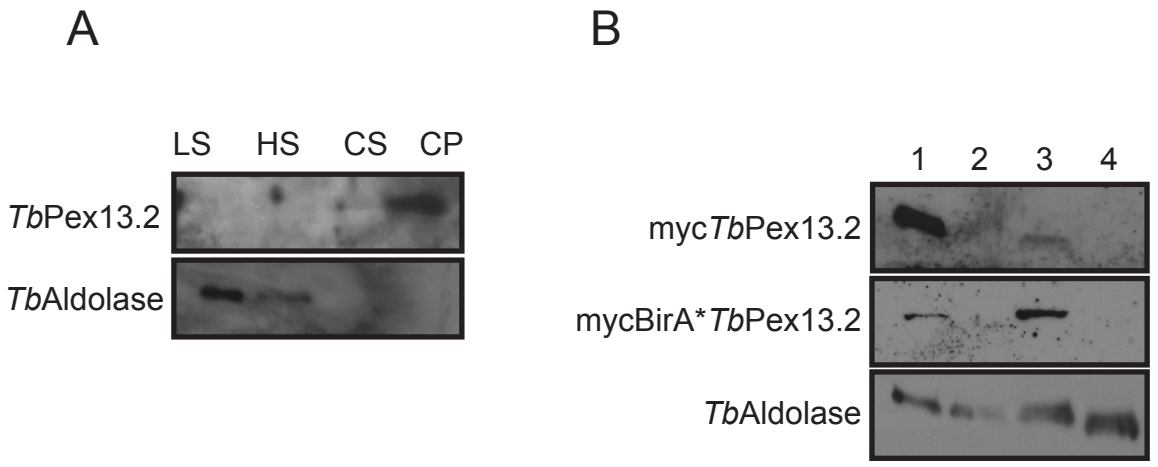
A
LS
HS
CS
CP
TbPex13.2
TbAldolase
B
1
2
3
4
mycTbPex13.2
mycBirA*TbPex13.2
TbAldolase

Figure 4

A

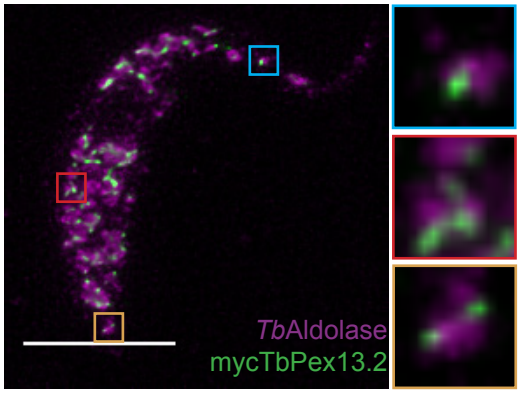

B

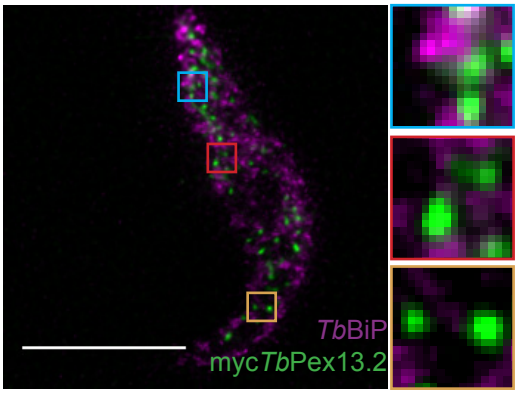

C

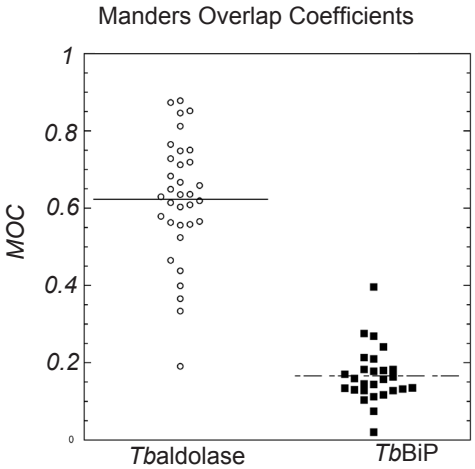

D

	*Tb*aldolase	*Tb*BiP
MOC	0.62 ± 0.16	0.17 ± 0.07
M1	0.49 ± 0.20	0.14 ± 0.14
M2	0.91 ± 0.10	0.38 ± 0.13

E

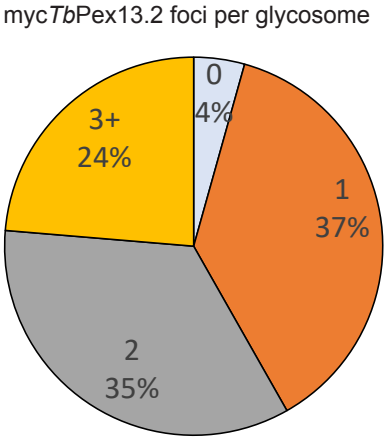

Figure 5

A

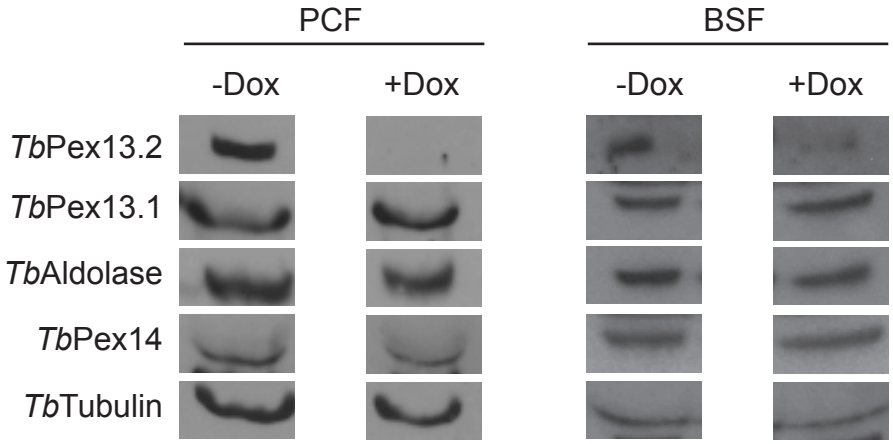
PCF
BSF
-Dox
+Dox
-Dox
+Dox
TbPex13.2
TbPex13.1
TbAldolase
TbPex14
TbTubulin

B

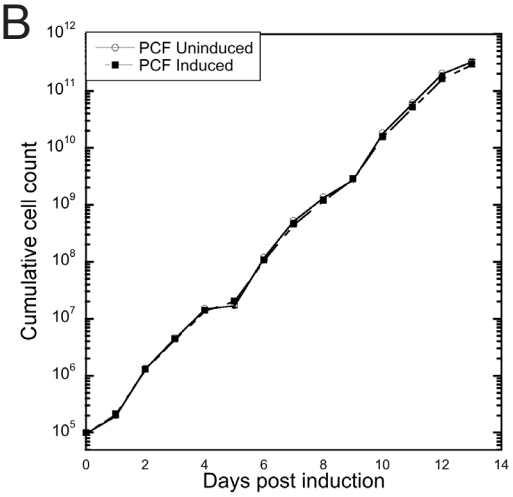
PCF Uninduced
PCF Induced
Cumulative cell count
Days post induction

C

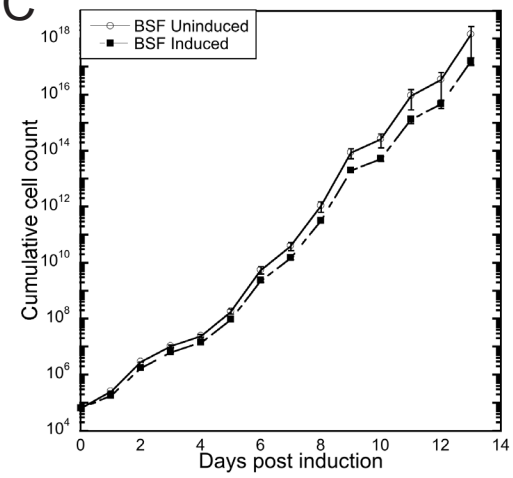
BSF Uninduced
BSF Induced
Cumulative cell count
Days post induction

Figure 6

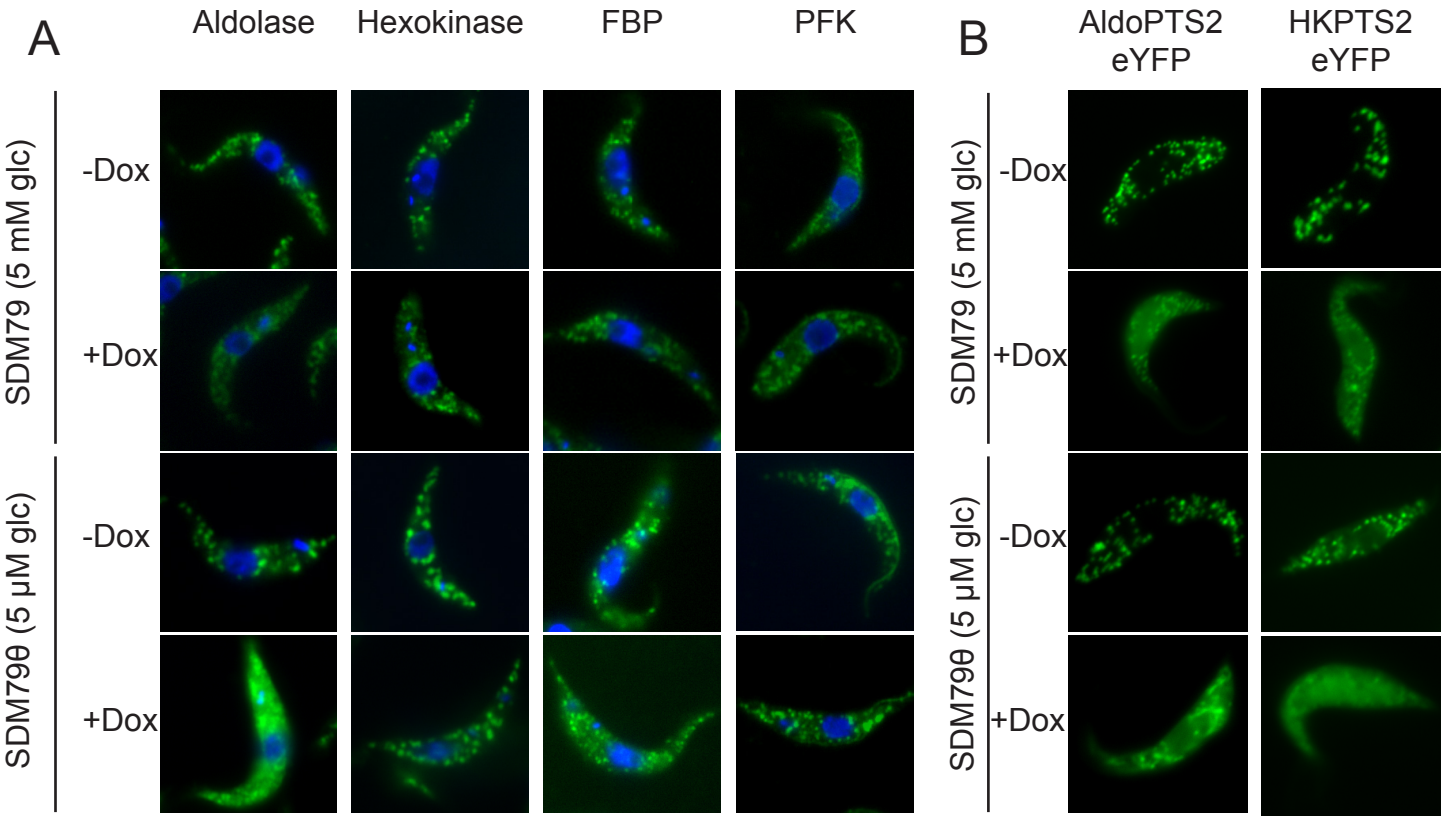
A
Aldolase
Hexokinase
FBP
PFK
SDM79 (5 mM glc)
-Dox
+Dox
SDM79θ (5 μM glc)
-Dox
+Dox
B
AldoPTS2 eYFP
HKPTS2 eYFP
SDM79 (5 mM glc)
-Dox
+Dox
SDM79θ (5 μM glc)
-Dox
+Dox

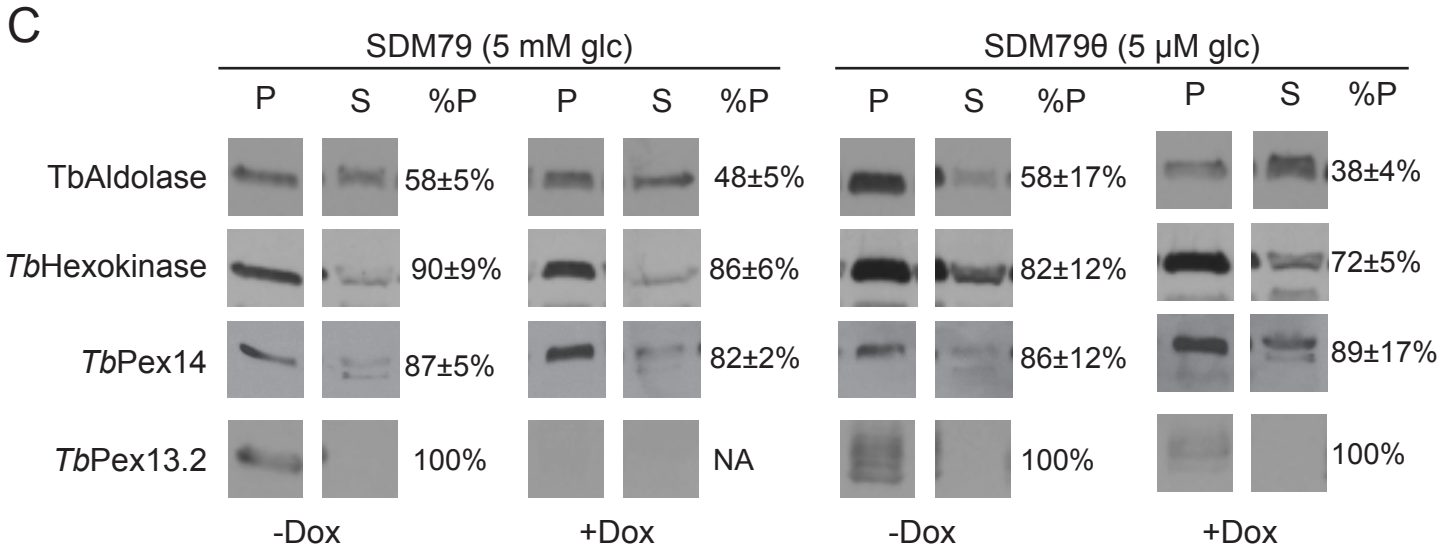
C
SDM79 (5 mM glc)
SDM79θ (5 μM glc)
P
S
%P
TbAldolase
58±5%
48±5%
58±17%
38±4%
*Tb*Hexokinase
90±9%
86±6%
82±12%
72±5%
*Tb*Pex14
87±5%
82±2%
86±12%
89±17%
*Tb*Pex13.2
100%
NA
100%
100%
-Dox
+Dox
-Dox
+Dox

Figure 7

A

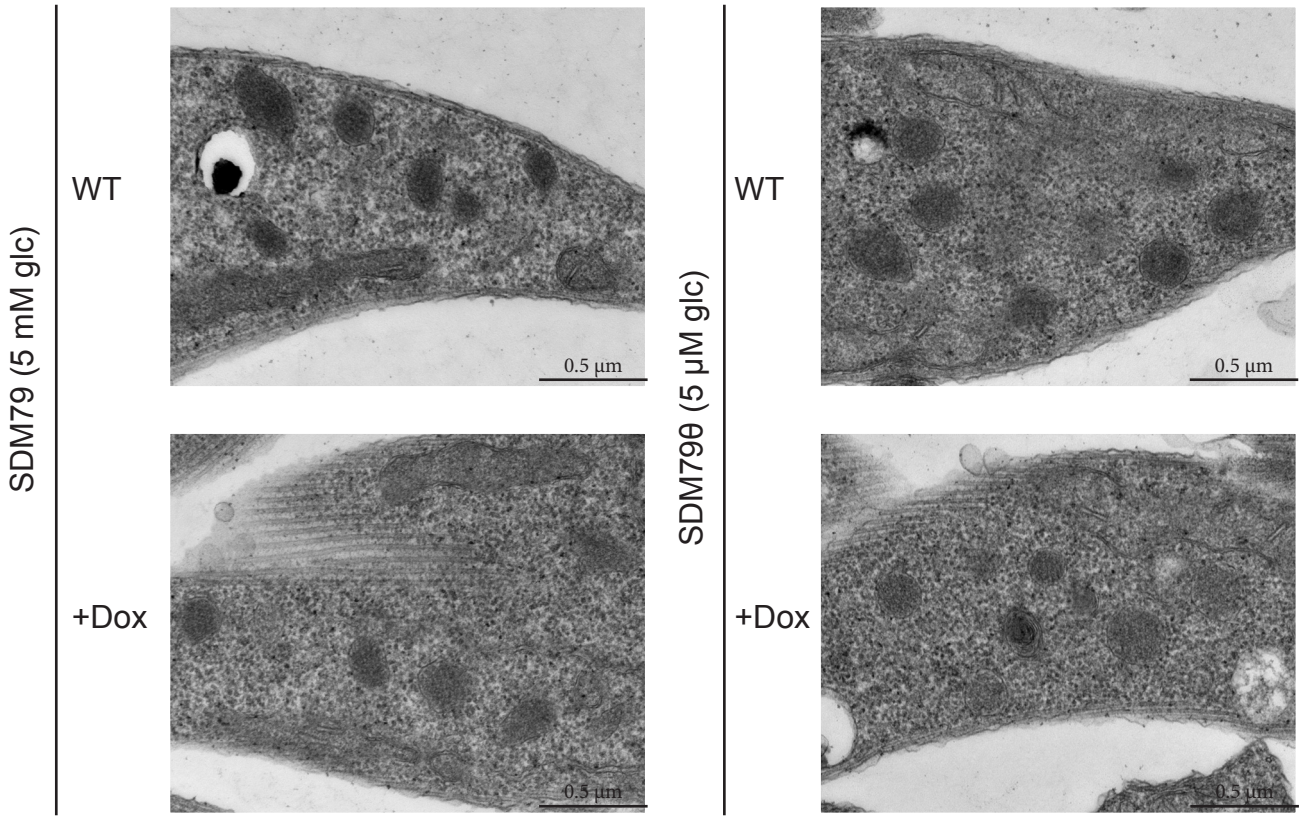
SDM79 (5 mM glc)
WT
+Dox
SDM79θ (5 µM glc)
WT
+Dox
0.5 µm
0.5 µm
0.5 µm
0.5 µm

B

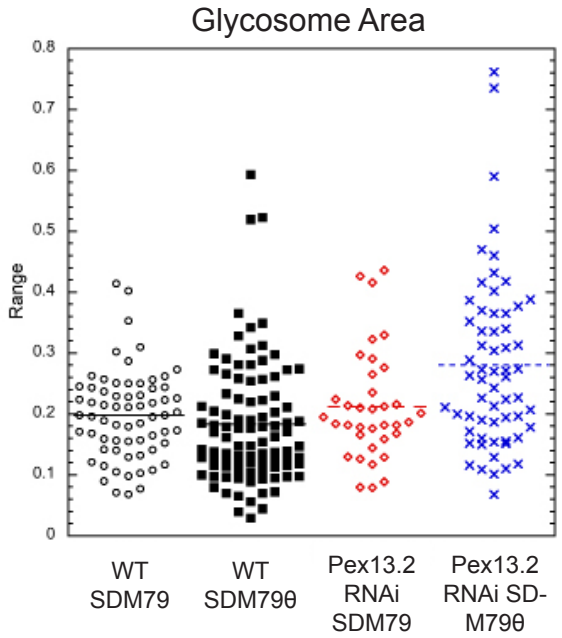
Glycosome Area
Range
0.8
0.7
0.6
0.5
0.4
0.3
0.2
0.1
0
WT SDM79
WT SDM79θ
Pex13.2 RNAi SDM79
Pex13.2 RNAi SD-M79θ

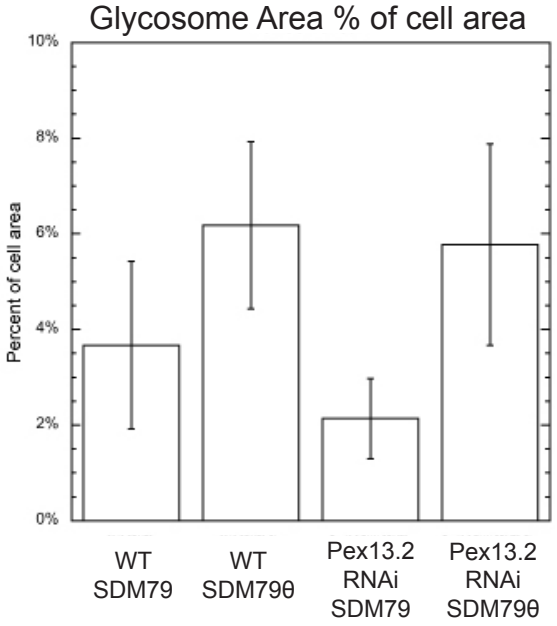
Glycosome Area % of cell area
Percent of cell area
10%
8%
6%
4%
2%
0%
WT SDM79
WT SDM79θ
Pex13.2 RNAi SDM79
Pex13.2 RNAi SDM79θ

Figure 8

A

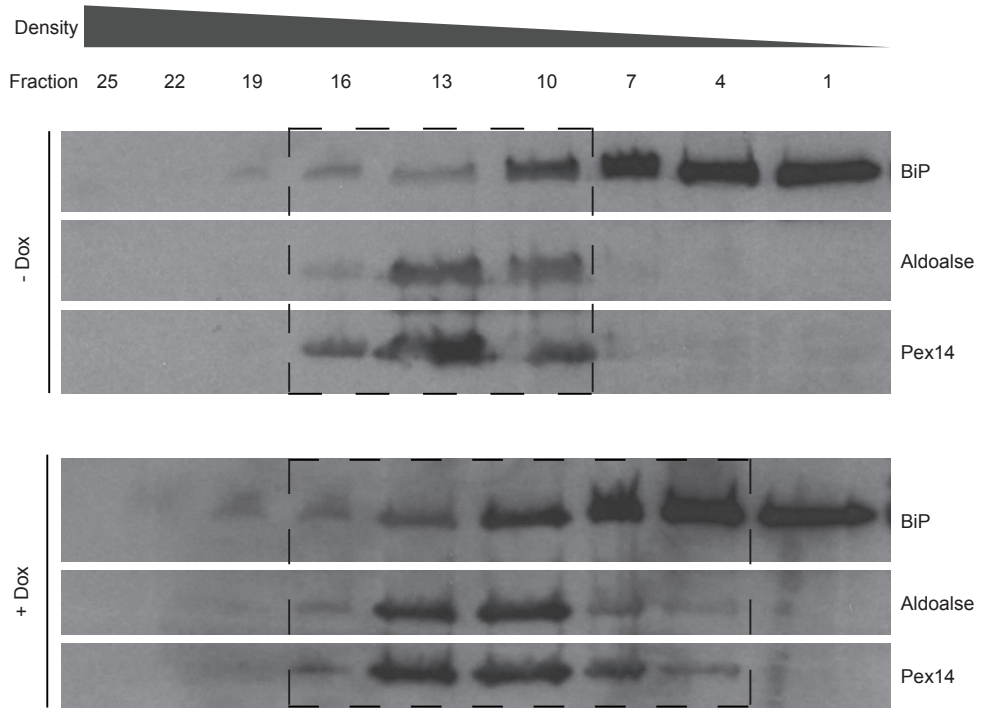
Density
Fraction 25 22 19 16 13 10 7 4 1
- Dox
BiP
Aldoalse
Pex14
+ Dox
BiP
Aldoalse
Pex14

B

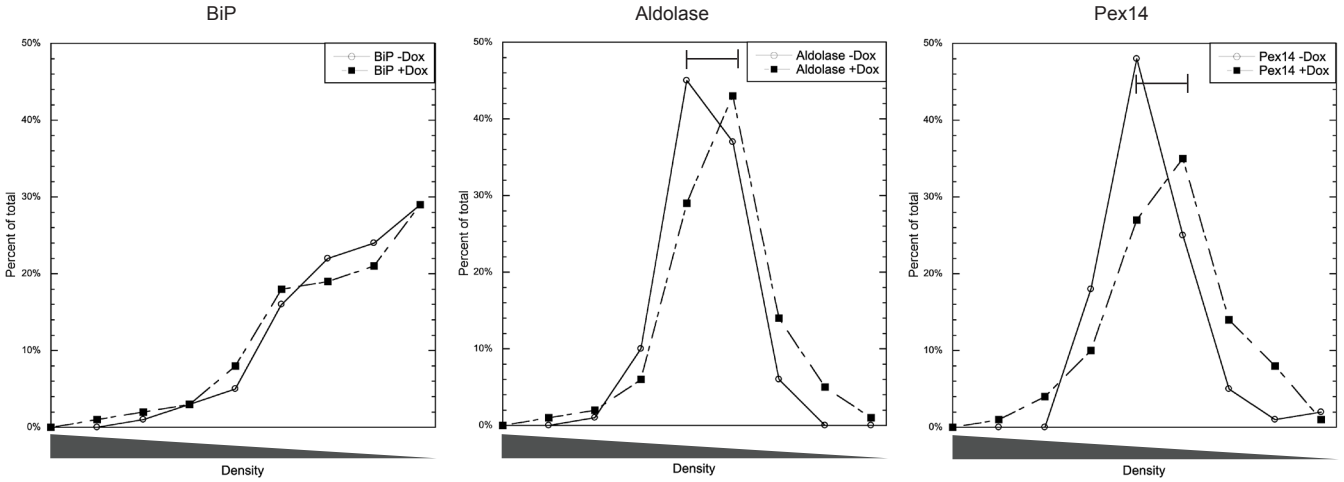
BiP
Aldolase
Pex14
BiP -Dox
BiP +Dox
Aldolase -Dox
Aldolase +Dox
Pex14 -Dox
Pex14 +Dox
Percent of total
0%
10%
20%
30%
40%
50%
Density
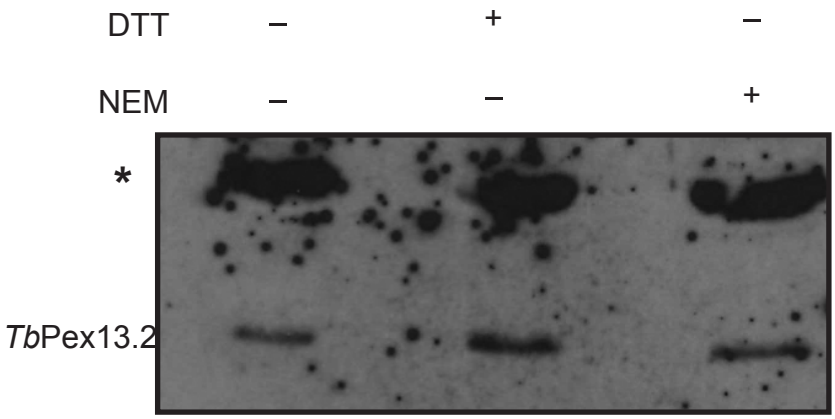
Figure S1